Int. J. Electrochem. Sci., 11 **(2016)** 7875 – 7889, doi: 10.20964/2016.09.34

International Journal of
ELECTROCHEMICAL
SCIENCE
www.electrochemsci.org

Bimetallic Ruthenium Vinyl Complexes Bridged by Electronic Substituent Phenylenes: Spectroelectrochemical and Computational Studies

Jing Zhang[1], *Chao-Fang Sun*[1], *Xiang-Hua Wu*[2], *Ming-Xing Zhang*[1], *Jun Yin*[1], *Guang-Ao Yu*[1], *Sheng Hua Liu*[1,*]

[1] Key Laboratory of Pesticide and Chemical Biology, Ministry of Education, College of Chemistry, Central China Normal University, Wuhan 430079, P.R. China
[2] College of Chemistry and Chemical Engineering, Yunnan Normal University, Kunming 650500, P.R. China
[*]E-mail: chshliu@mail.ccnu.edu.cn

Received: 29 January 2016 / *Accepted:* 4 July 2016 / *Published:* 7 August 2016

A combination of *in-situ* IR and UV/vis/NIR spectroelectrochemistry and DFT/TDDFT calculations have been employed to explore the spectroscopic and electronic properties of a series of dinuclear ruthenium vinyl complexes **1a**-**1d** $[RuCl(CO)(PMe_3)_3]_2(\mu$-CH=CH-Ar-CH=CH) (Ar = $C_6H_2(CH_3)_2$-2,5 (**1a**), $C_6H_2(OCH_3)_2$-2,5 (**1b**), $C_6H_2F_2$-2,5 (**1c**) and $C_6H_2(CF_3)_2$-2,5 (**1d**)). The spectroelectrochemical results combined with theoretical calculations reveal that there are no real electronic couplings between two ruthenium centers for **1a**-**1d** despite high half-wave potential splittings observed. The complexes **1a**-**1d** are characterized by localized oxidations of the bridging ligands and electron-releasing substituents render these localized oxidation processes more facile. In addition, the observed strong near-IR absorptions of $[\mathbf{1a}]^+$ and $[\mathbf{1b}]^+$ are mainly attributed to the metal-to-ligand charge-transfer (MLCT) transitions.

Keywords: Ruthenium Vinyl Complexes, Electronic Substituent, DFT Calculations, Phenylene Bridge.

1. INTRODUCTION

In recent years, the development of molecules in which two redox-active metal termini is attached to a common π-conjugated carbon bridge has aroused researchers' wide concern [1-14], because this family of molecules provide important model systems for exploiting intramolecular electron transfer, and their electronic and optical properties are of potential use in molecular scale

electronic materials and nanotechnological devices [15-20]. Among these complexes, 1,4-diethynylphenylene [21-30] and 1,4-divinylphenylene bridged [31-38] bimetallic complexes exhibit exceptional performances allowing for strong electronic interactions between two remote redox-active metal centers with extensive electron delocalization over the whole molecular frameworks. The evaluation for the electron-transfer abilities of the aforementioned systems is mainly base on a combination of electrochemical and spectroscopic techniques as well as a powerful supplement from the theoretical calculations. In this respect, we also have carried out some research [39] and reported a series of diruthenium complexes **1a-1d** bridged by 1,4-divinylphenylene unit bearing different donor and acceptor substituent groups (Scheme 1) [39]. But we just described their relevant syntheses and electrochemical studies and wasn't able to cover any spectroscopic and calculative studies to explore their electron-transfer essence because of the limitations of previous experimental conditions.

In our above work, the electrochemical results have revealed that complexes **1a-1d** all undergo two successive one-electron oxidation processes and their corresponding mixed-valence states exhibit high stability according to the pertinent wave splitting (ΔE) and thermodynamic equilibrium constant (K_c) values. Accordingly, the existence of stable oxidation species makes it possible to explore their electronic properties. In the present work, we will shed light on the real electron-transfer properties and mechanism of this series of bimetallic ruthenium vinyl complexes and get insight into how the introduction of different substituents mediates the electron-transfer processes, by employing *in-situ* IR and UV−vis−NIR spectroelectrochemical techniques as well as theoretical calculations.

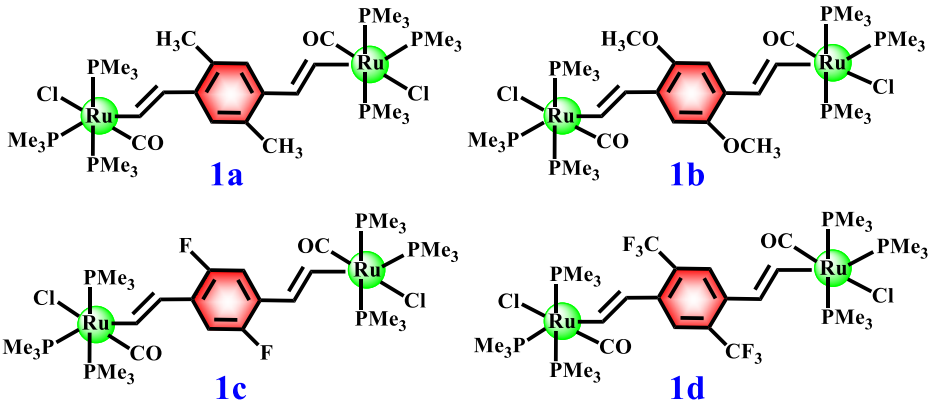

Scheme 1. Studied bimetallic ruthenium vinyl complexes **1a-1d**.

2. RESULTS & DISCUSSION

2.1 Electrochemical analysis

As reported in our previous work [39], complexes **1a-1d** and the unsubstituted reference complex **1e** ($[RuCl(CO)(PMe_3)_3]_2(\mu$-CH=CH-$C_6H_4$-CH=CH) all underwent two successive one-electron oxidation processes. When changing the substituent from electron-releasing group to electron-

withdrawing group, the values of the first oxidation potential E_1 increased gradually in the following order: 0.10 V (**1b**), 0.20 V (**1a**), 0.41 V (**1c**) and 0.57 V (**1d**) (Table 1). Accordingly, it's much easier to remove one electron from the more electron-rich systems of **1a** and **1b**. Furthermore, the wave separations (ΔE) increased in the same sequence: **1d** < **1c** < **1e** < **1a** < **1b** (Table 1). And an approximate linear correlation between the ΔE values and the σ_p Hammett constant [40] of the respective substituents can be observed (Figure S1), suggesting that the more electron-rich the bridging ligand is, the more stable the corresponding oxidation species may be. This rule is also observed in the following spectroelectrochemical experiments.

Table 1. Electrochemical data for complexes **1a-1d**[a]

Complex	E_1 (V)	E_2 (V)	ΔE (V)
1a	0.20	0.50	0.30
1b	0.10	0.46	0.35
1c	0.41	0.64	0.23
1d	0.57	0.75	0.18
1e	0.30	0.59	0.29

[a] Reference 22.

2.2 UV−Vis−NIR Spectroelectrochemistry

Table 2. UV−vis−NIR electronic absorption of diruthenium complexes **1a-1d** in various oxidation states (0, +1, +2).

Complex	λ_{max} (nm) (ε_{max} (dm^3 mol^{-1} cm^{-1}))
1a	317 (14983), 343 (15595)
$[\mathbf{1a}]^+$	300 (5882), 330 (5264), 513 (8449), 573 (10623), 993 (5264), 1134 (10235)
$[\mathbf{1a}]^{2+}$	340 (7259) , 392 (6452)
1b	299 (7885), 363 (12285)
$[\mathbf{1b}]^+$	355 (5846), 523 (4702), 577 (6782), 935 (2910), 1067 (4743)
$[\mathbf{1b}]^{2+}$	358 (7612)
1c	294 (7949), 356 (14886)
$[\mathbf{1c}]^+$	287 (5689), 359 (8455), 527 (1467), 583 (1720) , 1052 (1017), 1259 (1821)
$[\mathbf{1c}]^{2+}$	287 (5248), 392 (8121)
1d	352 (13160)
$[\mathbf{1d}]^+$	394 (7053)
$[\mathbf{1d}]^{2+}$	297 (3977)

In order to get direct information on the electron transfer properties of **1a-1d**, we conducted spectroelectrochemical studies within an optically transparent thin-layer electrochemical (OTTLE) cell, using dichloromethane/0.1 M *n*-Bu_4NPF_6 as the supporting electrolyte. The complexes **1a-1d**

were oxidized by increasing the potentials step by step (step width: 10, 20, or 30 mV). Spectral changes in the UV−vis−NIR region are presented in Figure 1 and Figures S2-S4 (Supporting Information). The relevant spectroscopic data are collected in Table 2.

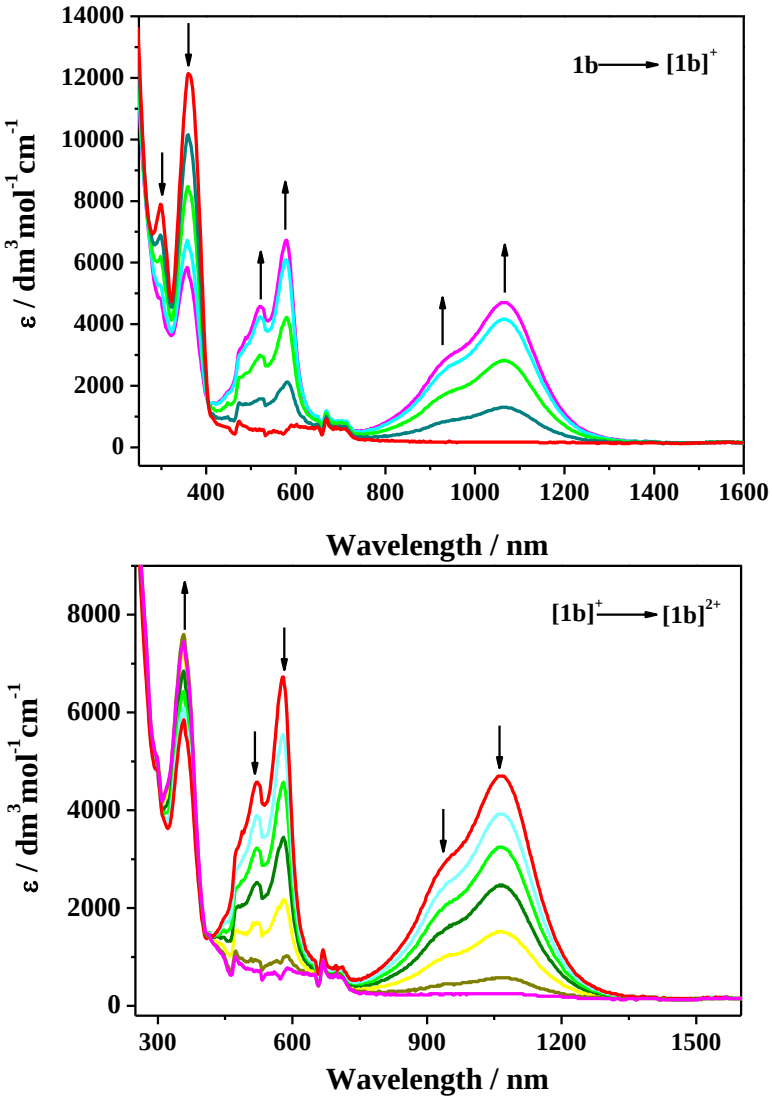

Figure 1. UV−Vis−NIR spectral changes recorded during the oxidation **1b**→[**1b**]$^{+}$ (top) and [**1b**]$^{+}$→[**1b**]$^{2+}$ (bottom) in $CH_2Cl_2/10^{-1}$ M *n*-Bu_4NPF_6 at 298 K within an OTTLE cell.

As shown in Figures 1 (**1b**) and S2-S4 (**1a**, **1c** and **1d**), the neutral **1a-1d** all exhibited intense absorption peaks in UV region, which can be mainly ascribed to intraligand centered transitions mixed with some MLCT contributions. When oxidized to cationic [**1a**]$^{+}$-[**1c**]$^{+}$, the intensity of the original bands decreased gradually, while a set of twin peaks between 510 nm and 580 nm and conspicuous absorptions in the near-IR region appeared simultaneously. These alterations are similar to those observed of the related reported complexes [32-35, 41, 42]. The distinct NIR absorptions are mainly attributed to transitions of MLCT (from metal to bridging ligand) on the basis of TDDFT calculations (vide infra), and further can be deconvoluted into the sum of two Gaussian-shaped sub-bands (Figure 2, Figure S5 and Table 3). By analyzing the related data, the introduction of the electron-donating groups stabilizes the mono-cationic states [**1a**]$^{+}$ and [**1b**]$^{+}$ relative to [**1c**]$^{+}$, causing the energy of the v_1

and v_2 transitions higher-shifted (Table 3). Regarding the two steps of one-electron oxidations of **1d**, the absorption in the UV region just decreased gradually and no notable NIR absorption could be observed in its monocationic state (Figures S4). The above observation is probably due to rapid decomposition of the unstable cationic **1d**$^+$, also in agreement with the irreversible nature of its anodic cyclic voltammogram [39]. On further oxidation to [**1a**]$^{2+}$-[**1c**]$^{2+}$, the characteristic absorption bands at around 500 nm and in the NIR region disappeared, accompanied by some changes of the absorptions in the UV region.

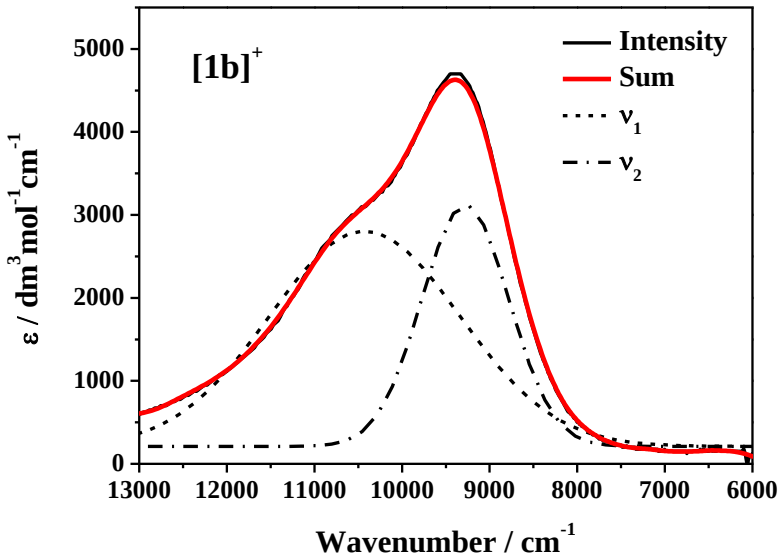

Figure 2. Deconvolution of the NIR absorptions of [**1b**]$^+$ by using two Gaussian-shaped bands, as determined by spectroelectrochemistry in an OTTLE cell.

Table 3. Selected parameters derived from deconvolution of the NIR absorption band envelope in [**1a**]$^+$-[**1c**]$^+$.[a]

Complex	[**1a**]$^+$	[**1b**]$^+$	[**1c**]$^+$
v_1/cm^{-1} (ε_{max}/ L mol^{-1} cm^{-1})	9834 (5345)	10426 (2595)	9402 (615)
v_2/cm^{-1} (ε_{max}/ L mol^{-1} cm^{-1})	8701 (6994)	9278 (2917)	7968 (1278)
$\Delta(v_1)_{1/2}$[b]	2425	2169	1179
$\Delta(v_2)_{1/2}$[b]	993	996	1159

[a] Samples generated in an OTTLE cell from solutions in CH_2Cl_2/0.1 M *n*-Bu_4NPF_6, with apparent molar absorption coefficients, ε. [b] $\Delta(v_1)_{1/2}$ is the observed half-height bandwidth.

2.3 IR Spectroelectrochemistry

IR spectroelectrochemistry was also exploited to determine the nature of the oxidation for complexes **1a-1d** by monitoring the evolution of the characteristic strong carbonyl stretching vibrations during the oxidation processes. Therefore, the related experiments were carried out within the OTTLE cell at room temperature (Figure 3). The pertinent data are collected in Table 4.

The neutral **1a-1d** each show a single ν(C≡O) band at about 1920 cm^{-1}, which is consistent with analogous electron densities at two ruthenium centers and extent of the Ru-to-CO fragment. Gradual oxidation to $[\mathbf{1a}]^{+}$-$[\mathbf{1d}]^{+}$ caused some decreases in intensities of the ν(C≡O) bands, but no obvious shifts can be observed. This observations also suggest that the electron densities of two Ru—CO segments in the oxidized forms resemble those in their corresponding neutral states. But the ν(C≡O) alterations of $[\mathbf{1d}]^{+}$ both in the intensity and position are the most noticeable, which coincides well with a greater contribution from the ruthenium centers to the spin density in DFT calculations. Further oxidation to the dicationic $[\mathbf{1a}]^{2+}$-$[\mathbf{1d}]^{2+}$ exhibited interesting differences from those of their corresponding monocations. The ν(C≡O) positions of $[\mathbf{1a}]^{2+}$-$[\mathbf{1c}]^{2+}$ all shifted towards much higher energy (more than 10 cm^{-1}), and the shift of $[\mathbf{1b}]^{2+}$ is the most obvious up to 15 cm^{-1}. Base on the above observations, we can speculate that the first step of oxidations for **1a-1d** probably localize more on the bridging ligands, affecting the Ru—CO bonds to a very limited extent, while the second steps are mainly concentrated on the metal centers and less on the phenylene-vinyl units.

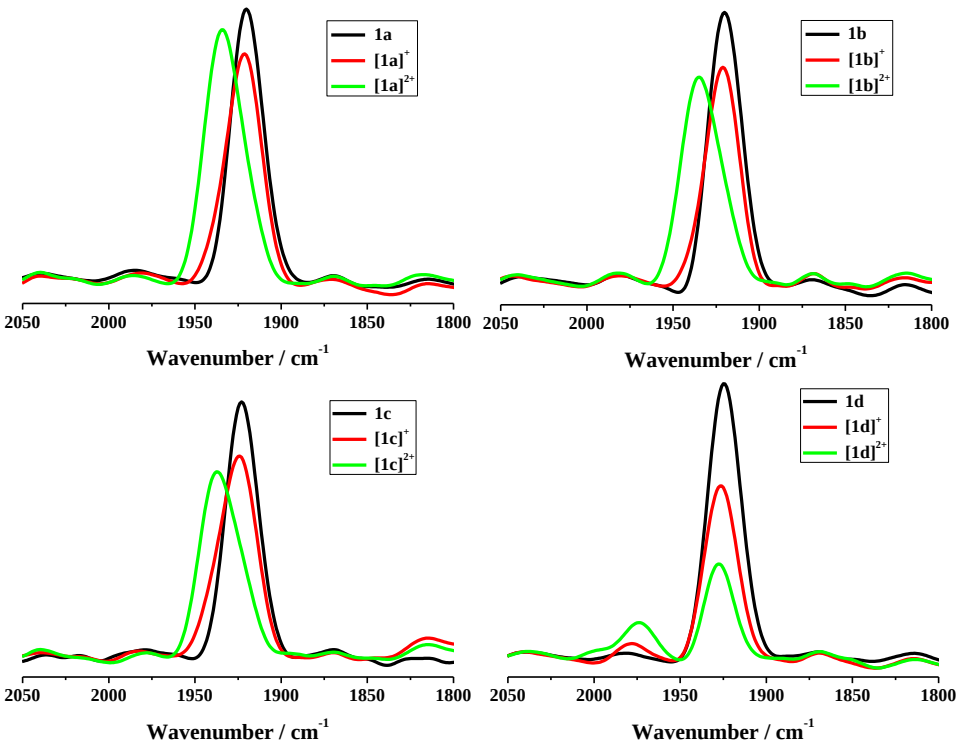

Figure 3. IR spectra recorded in the ν(C≡O) region for complexes **1a-1d** in different oxidation states (0, +1, +2) generated in $CH_2Cl_2/10^{-1}$ M *n*-Bu_4NPF_6 within an OTTLE cell at 298 K.

Table 4. Spectroelectrochemically determined ν(C≡O) wavenumbers (cm^{-1}) for $[\mathbf{1a}]^{n+}$- $[\mathbf{1d}]^{n+}$

Complex	n = 0	n = 1	n = 2
$[\mathbf{1a}]^{n+}$	1920	1921	1935
$[\mathbf{1b}]^{n+}$	1920	1921	1935
$[\mathbf{1c}]^{n+}$	1923	1924	1937
$[\mathbf{1d}]^{n+}$	1925	1926	1927, 1974

2.4 DFT and TD-DFT Calculations

A theoretical study was carried out in order to get insight into the electronic characters of [**1a**]$^+$-[**1d**]$^+$. We conducted density functional theory (DFT) calculations on representative and non-truncated model complexes [**1b**]$^+$ and [**1d**]$^+$, using the global hybrid functional B3LYP [43, 44] with a suitable continuum solvent model (CPCM, dichloromethane). The basis set employed was 6-31G* [45] (Lanl2dz for Ru atom) [46, 47]. Selected orbitals of [**1b**]$^+$ and [**1d**]$^+$ are presented in Figure 5. The frontier relevant molecular orbital energies and compositions for [**1b**]$^+$ and [**1d**]$^+$ from Mulliken analysis have been collected in Tables S1 (Supporting Information).

The spin densities of [**1b**]$^+$ and [**1d**]$^+$ are delocalized throughout the entire molecular backbones, revealing redox non-innocent characters of the bridging ligands (Figure 4). But some differences between these two complexes can be observed in terms of comparative analysis of their spin-density distributions. Obviously, [**1b**]$^+$ exhibits an uneven spin density distribution and the spin density concentrates almost entirely on the phenylene divinyl linker with only minor contributions from the metal centers. While the share from the bridging ligand in [**1d**]$^+$ is slightly smaller than that in [**1b**]$^+$, with a larger contribution from the metal moiety. It should be noted that the spin density in [**1b**]$^+$ also delocalizes onto the strong electron-releasing substituent (—OMe), but the electron-withdrawing group (—CF_3) of [**1d**]$^+$ makes no any contribution to the distribution. The above results clearly demonstrate that the introduction of electron-releasing substituent is favorable for the oxidation process and increases the involvement of the bridging ligand, which is also reflected by the experimental (both cyclic voltammetric and spectroelectrochemical) observations.

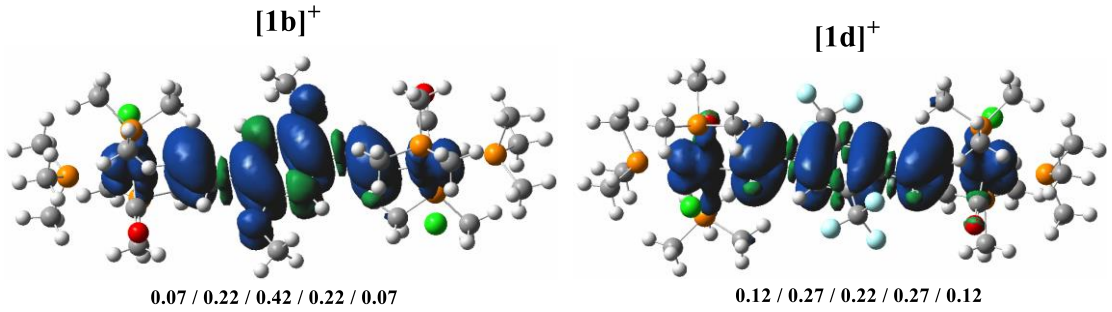

Figure 4. Spin-density distributions in [**1b**]$^+$ and [**1d**]$^+$ (Ru/CH=CH/Ar/CH=CH/Ru) with the corresponding compositions. Contour values: ±0.04 $(e/bohr^3)^{1/2}$.

The electronic transitions were also determined by time-dependent (TD) DFT calculations on models of the oxidized complexes [**1b**]$^+$ and [**1d**]$^+$ to help the assignment of the optical absorptions in the oxidized species. The predicted major electronic excitation information have been depicted in Figure 5 and Table 5. For [**1d**]$^+$, the simulation of the absorption in the NIR region is not consistent with the absent NIR absorption in the recorded spectrum of [**1d**]$^+$, so we just presented the UV absorptions of [**1d**]$^+$ in Table 5. This discrepancy may signify that the DFT calculations exaggerate the delocalization in some extent. The transition at 493 nm (20284 cm^{-1}) of [**1d**]$^+$ coming from α-HOSO→α-LUSO and β-HOSO-10→β-LUSO exhibits an intense metal-to-ligand (ML) CT and some bridge intraligand π-π* characters. With regard to [**1b**]$^+$, the main bands observed experimentally,

especially the low-energy absorptions in the NIR region (Table 5 and Figure 5), have been well predicted though with some higher-energy shifts. The lowest-energy excitation at 851 nm (11751 cm^{-1}) for $[\mathbf{1b}]^+$ is associated with β-HOSO→β-LUSO and α-HOSO→α-LUSO excitations, both being mainly attributed to intraligand π→π* transitions with an important metal-to-ligand (ML) CT component, which can be assigned to the observed broad NIR transition, namely v_1, as identified by Gaussian deconvolution in Figure 2.

Table 5. Major electronic excitations in $[\mathbf{1b}]^+$ and $[\mathbf{1d}]^+$ determined by TD-DFT methods.[a]

Complex	λ/nm [cm^{-1}]	Osc. str (*f*)	Major contributions	Assignment
$[\mathbf{1b}]^+$	851 [11751]	0.5051	β-HOSO→β-LUSO (97%) α-HOSO→α-LUSO (22%)	MLCT / ILCT
	709 [14104]	0.0001	β-HOSO-2→β-LUSO (99%)	MLCT/ L(auxiliary)MCT
	605 [16529]	0.0012	β-HOSO-5→β-LUSO (99%)	MLCT/ L(auxiliary)MCT
	528 [18939]	0.1269	β-HOSO-7→β-LUSO (88%)	ILCT / MLCT
	485 [20619]	0.9403	α-HOSO→α-LUSO (80%)	π-π* / ILCT
$[\mathbf{1d}]^+$	493 [20284]	0.7396	α-HOSO→α-LUSO (79%) β-HOSO-10→β-LUSO (35%)	π-π* / ILCT

[a] The computation method is B3LYP / 6-31G* (Ru: Lanl2DZ) / CPCM / CH_2Cl_2. *D* = doublet.

The other excitations in higher energies are all related to the involvements of the metal centers, the bridges and auxiliary ligands, but they are not involved in the direct electron transfer between two metal ruthenium centers. This means that there are no real electronic couplings between two ruthenium centers despite high half-wave potential splittings as Winter and co-workers reported [42], and the singly oxidized species really show some MLCT, ILCT or LMCT transitions for **1b**. The above theoretical results confirm that two anodic steps of electron transfer authentically occur between the central linker and one end of two metal frameworks but not two metal centers in **1a-1d**, in line with the significant contributions of the bridging ligands even of the electron-releasing substituents in the preceding spin-density section. It must be noted that there are some discrepancies between the calculated absorptions and the experimental observations, which may be caused by the exaggerated delocalization of the DFT calculations. In addition, we cannot exclude the mutual impact of different conformers on the electron delocalization and localization [48-52].

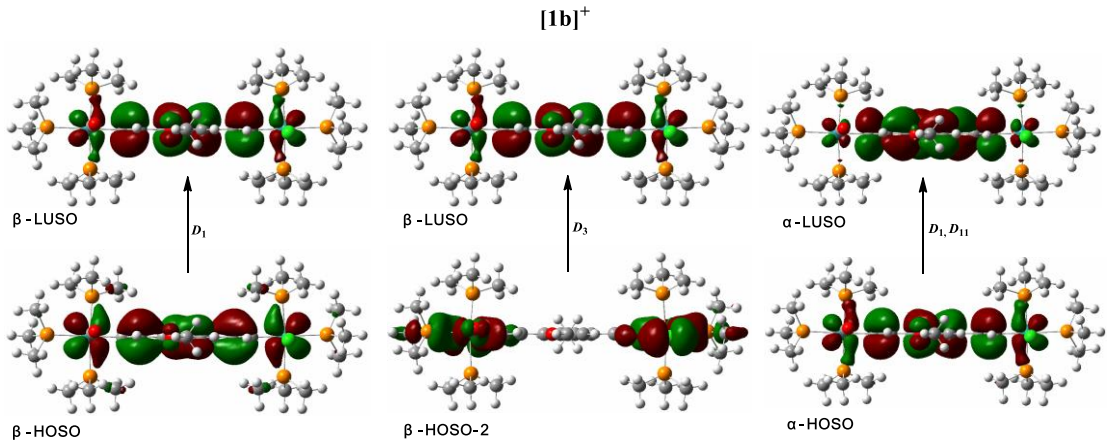

Figure 5. Spin orbitals involved in the major electronic excitations in [**1b**]$^+$ shown in **Table 5** (*D* = doublet). B3LYP / 6-31G* (Ru: Lanl2DZ) / CPCM / CH_2Cl_2.

3. EXPERIMENTAL

Physical Measurements. Spectroelectrochemical experiments at room temperature were performed with an airtight optically transparent thin-layer electrochemical (OTTLE) cell (optical path length of ca 200 μm) equipped with a Pt minigrid working electrode and CaF_2 windows [53]. The cell was positioned in the sample compartment of a Bruker Tensor FT-IR spectrometer (1 cm^{-1} spectral resolution, 8 scans) or a Shimadzu UV-3600 UV-Vis-NIR spectrophotometer. The controlled-potential electrolyses were carried out with a CHI 660C potentiostat. The concentration of samples was ca 2×10^{-3} mol dm^{-3}. Dry 10^{-1} M *n*-Bu_4NPF_6 was used as the supporting electrolyte.

Computational Details. DFT calculations were performed with the Gaussian 09 program [54], at the B3LYP/6-31G* levels of theory. Geometry optimizations were performed without any symmetry constraints, and frequency calculations on the resulting optimized geometries showed no imaginary frequencies. Electronic transitions were calculated by the time-dependent DFT (TD-DFT) method. The MO contributions were generated using the Multiwfn2.6.1_bin_Win package and plotted using GaussView 5.0. The solvation effects in dichloromethane are included for a part of the calculations with the conductor-like polarizable continuum model (CPCM) [55, 56].

4. CONCLUSIONS

The spectroscopic and electronic properties of a series of dinuclear ruthenium vinyl complexes **1a-1d** in different oxidation states have been explored by the *in-situ* IR and UV/vis/NIR spectroelectrochemistry and DFT/TDDFT calculations. The UV/vis/NIR spectroelectrochemical results reveal that the mono-cationic [**1a**]$^+$ and [**1b**]$^+$ with electron-releasing substituents all exhibit characteristic stronger absorption bands in the NIR region, compared with the complexes [**1c**]$^+$ and [**1d**]$^+$ with electron-withdrawing groups. In the IR spectroelectrochemical experiments of **1a-1d**, unconspicuous shifts of the *ν*(C≡O) absorptions during the first step of oxidations but remarkable

changes in the second steps demonstrate that the first step of oxidations localize on the bridge ligands, while the second steps are largely concentrated on the metal centers. Furthermore, the DFT and TD-DFT calculations show that the electron-donating substituents promote the localized oxidations of the bridging ligands but not the metal termini, and there are no real electronic couplings between two ruthenium centers despite high half-wave potential splittings observed. Therefore, our findings may have general implications in the exploration of electron transfer process for new molecular wires in the electron devices field.

Notes

The author declares no competing financial interest.

ACKNOWLEDGEMENTS

The authors acknowledge financial support from National Natural Science Foundation of China (21272088, 21472059, 21402057), the self-determined research funds of CCNU from the colleges' basic research and operation of MOE (CCNU14A05009, CCNU14F01003) and the excellent doctorial dissertation cultivation grant from Central China Normal University (2015YBYB108).

† Electronic supplementary information (ESI) available: Electrochemical, UV−Vis−NIR and calculated DFT data.

Electrochemistry

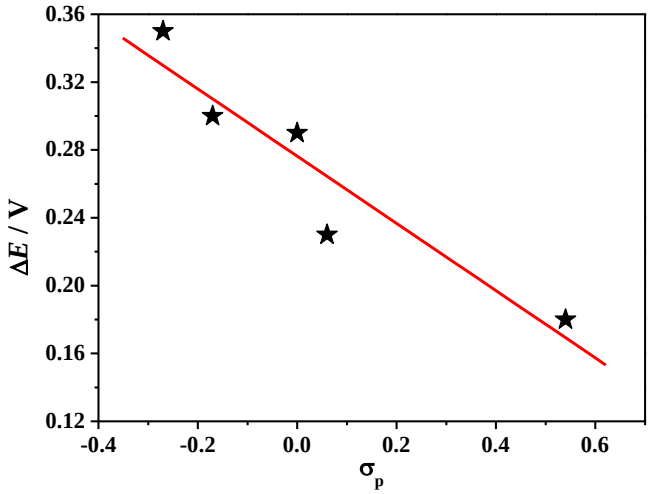

Figure S1. Correlation of the Δ*E* values and the σ_p Hammett constant of the substituents, linear fit (R^2=0.89, red line).

UV−Vis−NIR Spectroelectrochemistry

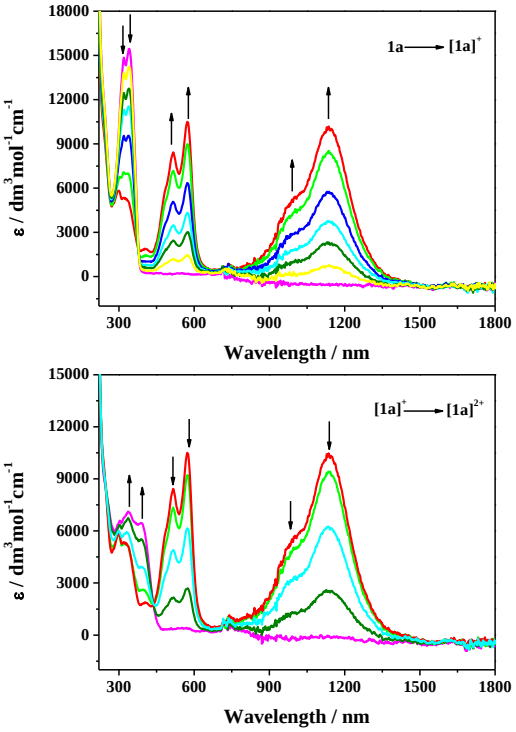

Figure S2. UV−vis−NIR spectral changes recorded during the oxidation **1a**→[**1a**]$^{+}$ (top) and [**1a**]$^{+}$→[**1a**]$^{2+}$ (bottom) in CH_2Cl_2/10^{-1} M *n*-Bu_4NPF_6 at 298 K within an OTTLE cell.

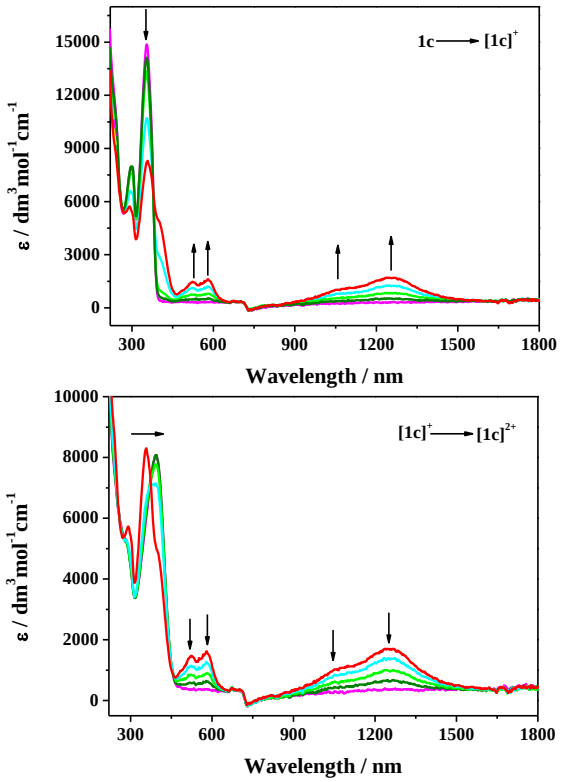

Figure S3. UV−vis−NIR spectral changes recorded during the oxidation **1c**→[**1c**]$^{+}$ (top) and [**1c**]$^{+}$→[**1c**]$^{2+}$ (bottom) in CH_2Cl_2/10^{-1} M *n*-Bu_4NPF_6 at 298 K within an OTTLE cell.

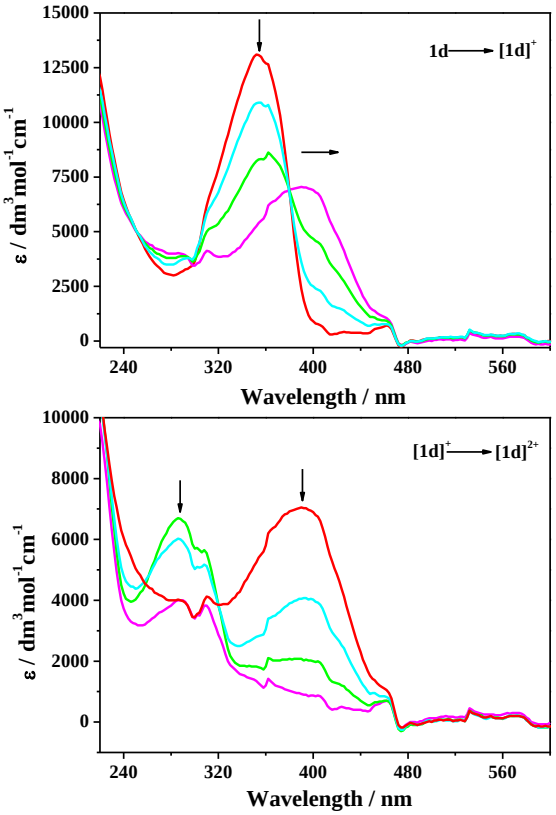

Figure S4. UV−vis spectral changes recorded during the oxidation **1d**→[**1d**]$^{+}$ (top) and [**1d**]$^{+}$→[**1d**]$^{2+}$ (bottom) in CH_2Cl_2/10^{-1} M *n*-Bu_4NPF_6 at 298 K within an OTTLE cell.

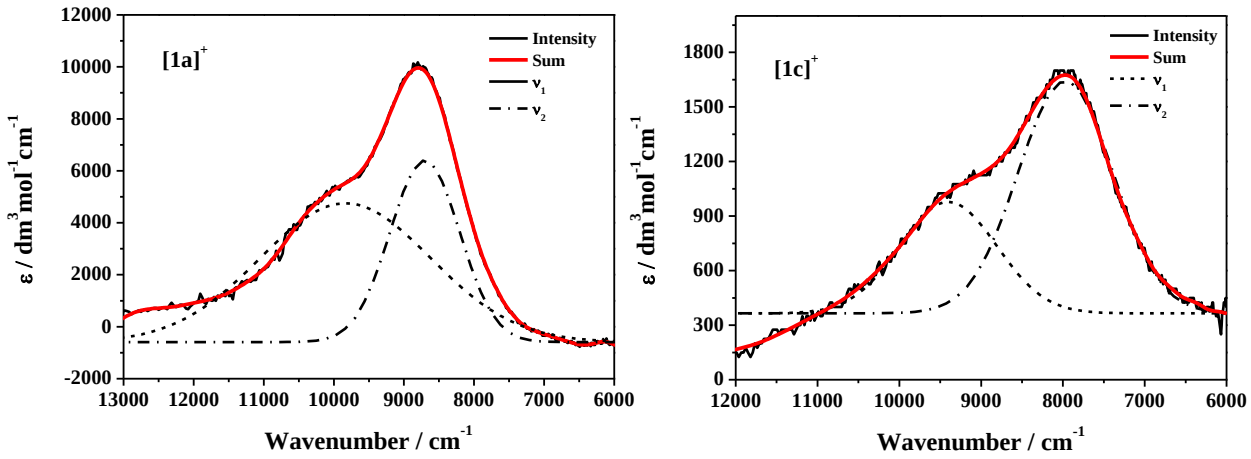

Figure S5. Deconvolutions of the NIR absorptions of [**1a**]$^{+}$ and [**1c**]$^{+}$ by using two Gaussian-shaped bands, as determined by spectroelectrochemistry in an OTTLE cell.

DFT Calculations

Table S1. Energy and composition of frontier molecular orbitals of the model complexes [**1b**]$^+$ and [**1d**]$^+$. B3LYP / 6-31G* (Ru: Lanl2DZ) / CPCM / CH_2Cl_2.

	MO		eV	(CO)1	Cl1	$(PMe_3)_3$1	Ru1	(C=C)1	Ar	(C=C)2	Ru2	$(PMe_3)_3$2	Cl2	(CO)2
[**1b**]$^+$	β223	β-LUSO	-3.99	0	0	0	6	20	48	20	6	0	0	0
	β217	β-H-5	-6.60	2	29	6	13	0	0	0	13	6	29	2
	β215	β-H-7	-7.00	3	1	15	19	3	18	3	19	15	1	3
[**1d**]$^+$	α240	α-LUSO	-2.34	0	0	0	3	19	56	19	3	0	0	0
	α239	α-HOSO	-5.81	0	0	0	12	21	34	21	12	0	0	0
	β239	β-LUSO	-4.49	0	0	0	10	13	54	13	10	0	0	0
	β228	β-H-10	-7.67	2	17	1	11	2	34	2	11	1	17	2

References

1. A. Ceccon, S. Santi, L. Orian and A. Bisello, *Coord. Chem. Rev*., 248 (2004) 683.
2. F. Barigelletti and L. Flamigni, *Chem. Soc. Rev*., 29 (2000) 1.
3. S. Barlow and D. O'Hare, *Chem. Rev*., 97 (1997) 637.
4. P. F. H. Schwab, M. D. Levin and J. Michl, *Chem. Rev*., 99 (1999) 1863.
5. J. Zhang, M. X. Zhang, C. F. Sun, M. Xu, F. Hartl, J. Yin, G. A. Yu, L. Rao and S. H. Liu, *Organometallics*, 34 (2015) 3967.
6. A. Hildebrandt and H. Lang, *Organometallics*, 32 (2013) 5640.
7. G. L. Xu, R. J. Crutchley, M. C. DeRosa, Q.-J. Pan, H.-X. Zhang, X. Wang and T. Ren, *J. Am. Chem. Soc*., 127 (2005) 13354.
8. J. Zhang, C. F. Sun, M. X. Zhang, F. Hartl, J. Yin, G. A. Yu, L. Rao and S. H. Liu, *Dalton. Trans.*, 45 (2016) 768.
9. A. Irfan, S. Muhammad, A. G. Al-Sehemi, M. S. Al-Assiri and A. Kalam, *Int. J. Electrochem. Sci*., 10 (2015) 3600.
10. C.-J. Yao, Y.-W. Zhong and J. N. Yao, *J. Am. Chem. Soc*., 133 (2011) 15697.
11. C.-J. Yao, Y.-W. Zhong, H.-J. Nie, H. D. Abruña and J. N. Yao, *J. Am. Chem. Soc*., 133 (2011) 20720.
12. Y.-W. Zhong, Z.-L. Gong, J.-Y. Shao and J. N. Yao, *Coord. Chem. Rev*., 312 (2016) 22.
13. S. I. Al-Saeedi, A. M. Alsalme, A. Nafady, *Int. J. Electrochem. Sci*., 10 (2015) 2170.
14. B. Q. Yuan, Y. C. Zhu, K. Xu, *Int. J. Electrochem. Sci*., 10 (2015) 4138.
15. P. J. Low, *Coord. Chem. Rev*., 257 (2013) 1507.
16. J.-P. Launay, *Coord. Chem. Rev*., 257 (2013) 1544.
17. F. A. Saad, *Int. J. Electrochem. Sci*., 9 (2014) 4761.
18. P. Hamon, F. Justaud, O. Cador, P. Hapiot, S. Rigaut, L. Toupet, L. Ouahab, H. Stueger, J.-R. Hamon and C. Lapinte, *J. Am. Chem. Soc*., 130 (2008) 17372.
19. A. Taherpour, P. S. Lajevardi, *Int. J. Electrochem. Sci*., 6 (2011) 5482.
20. B. Q. Yuan, Y. C. Zhu and K. Xu, *Int. J. Electrochem. Sci*., 10 (2015) 4138.
21. L. Luo, A. Benameur, P. Brignou, S. H. Choi, S. Rigaut and C. D. Frisbie, *J. Phys. Chem. C*, 115 (2011) 1995.

22. C. Olivier, K. Costuas, S. Choua, V. Maurel, P. Turek, J.-Y. Saillard, D. Touchard and S. Rigaut, *J. Am. Chem. Soc*., 132 (2010) 5638.
23. S. Rigaut, C. Olivier, K. Costuas, S. Choua, O. Fadhel, J. Massue, P. Turek, J. Y. Saillard, P. H. Dixneuf and D. Touchard, *J. Am. Chem. Soc*., 128 (2006) 5859.
24. A. Klein, O. Lavastre and J. Fiedler, *Organometallics*, 25 (2006) 635.
25. N. Gauthier, N. Tchouar, F. Justaud, G. Argouarch, M. P. Cifuentes, L. Toupet, D. Touchard, J.-F. Halet, S. Rigaut, M. G. Humphrey, K. Costuas and F. Paul, *Organometallics*, 28 (2009) 2253.
26. L.-B. Gao, J. Kan, Y. Fan, L.-Y. Zhang, S.-H. Liu, Z.-N. Chen, *Inorg. Chem*., 46 (2007) 5651.
27. C. Olivier, B.-S. Kim, D. Touchard and S. Rigaut, *Organometallics*, 27 (2008) 509.
28. M. A. Fox, J. D. Farmer, R. L. Roberts, M. G. Humphrey and P. J. Low, *Organometallics*, 28 (2009) 5266.
29. M. I. Bruce, K. Costuas, B. G. Ellis, J.-F. Halet, P. J. Low, B. Moubaraki, K. S. Murray, N. Ouddai, G. J. Perkins, B. W. Skelton and A. H. White, *Organometallics*, 26 (2007) 3735.
30. J.-L. Xia, W. Y. Man, X. Zhu, C. Zhang, G. J. Jin, P. A. Schauer, M. A. Fox, J. Yin, G. A. Yu, P. J. Low and S. H. Liu, *Organometallics*, 31 (2012) 5321.
31. J. Zhang, Y. Ou, M. Xu, C. Sun, J. Yin, G. A. Yu and S. H. Liu, *Eur. J. Inorg. Chem*., (2014) 2941.
32. W. Y. Man, J.-L. Xia, N. J. Brown, J. D. Farmer, D. S. Yufit, J. A. K. Howard, S. H. Liu and P. J. Low, *Organometallics*, 30 (2011) 1852.
33. J. Maurer, B. Sarkar, W. Kaim, R. F. Winter and S. Záliš, *Chem. Eur. J*., 13 (2007) 10257.
34. J. Maurer, B. Sarkar, B. Schwederski, W. Kaim, R. F. Winter and S. Záliš, *Organometallics*, 25 (2006) 3701.
35. J. Maurer, R. F. Winter, B. Sarkar, J. Fiedler, S. Záliš, *Chem. Commun*., (2004) 1900.
36. X.-H. Wu, J. H. Liang, J. L. Xia, S. Jin, G. A. Yu, S. H. Liu, *Organometallics*, 29 (2010) 1150.
37. P. Mücke, M. Zabel, R. Edge, D. Collison, S. Clément, S. Záliš and R. F. Winter, *J. Organomet. Chem*., 696 (2011) 3186.
38. X. Wu, T. Weng, S. Jin, J. Liang, R. Guo, G. Yu and S. H. Liu, *J. Organomet. Chem*., 694 (2009) 1877.
39. X. H. Wu, S. Jin, J. H. Liang, Z. Y. Li, G.-A. Yu and S. H. Liu, *Organometallics*, 28 (2009) 2450.
40. C. Hansch, A. Leo and R. W. Taft, *Chem. Rev*., 91 (1991) 165.
41. R. F. Winter, *Organometallics*, 33 (2014) 4517.
42. Y.-P. Ou, J. Zhang, M. Xu, J. L. Xia, F. Hartl, J. Yin, G.-A. Yu, S. H. Liu, *Chem. Asian J*., 9 (2014) 1152.
43. A. D. Becke, *J. Chem. Phys*., 98 (1993) 5648.
44. C. Lee, W. Yang and R. G. Parr, *Phys. Rev. B*, 37 (1988) 785.
45. T. H. Dunning and P. J. Hay, in Modern Theoretical Chemistry, Vol. 3 (Ed.: H. F. Schaefer), Plenum, New York, (1976) 1.
46. P. J. Hay and W. R. Wadt, *J. Chem. Phys*., 82 (1985) 270.
47. P. J. Hay and W. R. Wadt, *J. Chem. Phys*., 82 (1985) 299.
48. M. Parthey, J. B. G. Gluyas, P. A. Schauer, D. S. Yufit, J. A. K. Howard, M. Kaupp and P. J. Low, *Chem. Eur. J*., 19 (2013) 9780.
49. M. Parthey and M. Kaupp, *Chem. Soc. Rev*., 43 (2014) 5067.
50. A. Burgun, F. Gendron, C. Sumby, T. Roisnel, O. Cador, K. Costuas, J.-F. Halet, M. I. Bruce and C. Lapinte, *Organometallics*, 33 (2014) 2613.
51. R. Makhoul, Y. Kumamoto, A. Miyazaki, F. Justaud, F. Gendron, J.-F. Halet, J.-R. Hamon and C. Lapinte, *Eur. J. Inorg. Chem*., (2014) 3899.
52. R. Makhoul, H. Sahnoune, V. Dorcet, J.-F. Halet, J.-R. Hamon and C. Lapinte, *Organometallics*, 34 (2015) 3314.
53. M. Krejčík, M. Daněk and F. Hart1, *J. Electroanal. Chem. Interfacial Electrochem*., 317 (1991) 179.

54. Gaussian 09, Revision D.01, M. J. Frisch, G. W. Trucks, H. B. Schlegel, G. E. Scuseria, M. A. Robb, J. R. Cheeseman, G. Scalmani, V. Barone, B. Mennucci, G. A. Petersson, H. Nakatsuji, M. Caricato, X. Li, H. P. Hratchian, A. F. Izmaylov, J. Bloino, G. Zheng, J. L. Sonnenberg, M. Hada, M. Ehara, K. Toyota, R. Fukuda, J. Hasegawa, M. Ishida, T. Nakajima, Y. Honda, O. Kitao, H. Nakai, T. Vreven, J. A. Montgomery, Jr., J. E. Peralta, F. Ogliaro, M. Bearpark, J. J. Heyd, E. Brothers, K. N. Kudin, V. N. Staroverov, R. Kobayashi, J. Normand, K. Raghavachari, A. Rendell, J. C. Burant, S. S. Iyengar, J. Tomasi, M. Cossi, N. Rega, J. M. Millam, M. Klene, J. E. Knox, J. B. Cross, V. Bakken, C. Adamo, J. Jaramillo, R. Gomperts, R. E. Stratmann, O. Yazyev, A. J. Austin, R. Cammi, C. Pomelli, J. W. Ochterski, R. L. Martin, K. Morokuma, V. G. Zakrzewski, G. A. Voth, P. Salvador, J. J. Dannenberg, S. Dapprich, A. D. Daniels, Ö. Farkas, J. B. Foresman, J. V. Ortiz, J. Cioslowski, D. J. Fox, Gaussian, Inc., Wallingford CT, 2009.
55. M. Cossi, N. Rega, G. Scalmani and V. Barone, *J. Comput. Chem.*, 24 (2003) 669.
56. V. Barone and M. Cossi, *J. Phys. Chem. A*, 102 (1998) 1995.